Catalytic Activity of Cu/SBA-15 for Peroxidation of Pyridine Bearing Wastewater at Atmospheric Condition

V. Subbaramaiah, Vimal Chandra Srivastava, and Indra Deo Mall
Dept. of Chemical Engineering, Indian Institute of Technology Roorkee, Roorkee, Uttarakhand 247667, India

DOI 10.1002/aic.14017
Published online February 19, 2013 in Wiley Online Library (wileyonlinelibrary.com)

In this study, Cu-loaded Santa Barbara amorphous (SBA)-15 catalysts were synthesized by impregnation method and further used for catalytic wet peroxidation (CWPO) of pyridine from aqueous solution using hydrogen peroxide as oxidant. The synthesized catalysts have been characterized by Brunauer–Emmett–Teller surface area: temperature-programmed reduction, H_2-chemisorption, Fourier transform infrared spectroscopy, and field emission scanning electron microscopy. Characterization results indicate good dispersion of Cu species inside the porous structure of SBA-15. The effect of various parameters such as Cu loading on SBA-15, pH, catalyst dose, H_2O_2 concentration, and temperature have been studied for their effect on CWPO of pyridine. More than 97% pyridine removal and 92% total organic carbon removal was achieved at optimum condition. Cu/SBA-15 showed stable performance during reuse for six cycles with negligible copper leaching. © 2013 American Institute of Chemical Engineers *AIChE J*, 59: 2577–2586, 2013
Keywords: wet peroxidation, catalytic oxidation, pyridine, Cu/SBA-15, mechanism

Introduction

Remediation of pyridine bearing wastewater is important owing to its large discharge during its usage and manufacturing in chemical, pharmaceuticals, and pesticide industries.[1] Pyridine is manufactured under extreme condition of temperature using ammonia, acetaldehyde, and so forth. During its manufacturing, huge amount of wastewater is generated from process industries which are highly recalcitrant and are, therefore, not submissive to biological treatment.[2] Exposure to pyridine causes harmful effects on liver, kidneys, immune systems, and reproductive functions, and it is a potential carcinogen.[1]

Several oxidation processes have been developed for the treatment of toxic organic compounds containing wastewater. Wet air oxidation is an attractive and powerful technique for treatment of high organic loading and nonbiodegradable wastewater into less harmful compounds such as CO_2, H_2O, and N_2.[3] Wet air oxidation is usually operated at elevated temperature (140–320°C) and at high pressure (5–20 bar) using pure oxygen or air as oxidant.[3,4] Because of severe reaction conditions of this process, there is an urgent need to develop economically eco-friendly and efficient routes to destroy toxic and/or refractory organic compounds from effluent streams to meet the discharge standards. Catalytic wet peroxidation (CWPO) is a promising alternative for the treatment of toxic and/or refractory wastewater streams under mild reaction conditions (<100°C temperature and at atmospheric pressure). CWPO mineralizes (i.e., complete conversion to CO_2 and H_2O) the organic compounds into less harmful and less toxic compounds.[5] These process involves the generation of highly reactive hydroxyl radical ($OH^{\bullet}$), which is one of the most powerful oxidizing agents.[6] The use of heterogeneous catalyst allows an easy separation and recovery of catalyst from the treated wastewater. Moreover, presence of a solid catalyst enhances the degradation rate due to the reactivity of organic compounds with active oxygenated species generated during hydrogen peroxide decomposition over the catalyst surface.[7]

Mesoporous silica materials were developed in 1990s, and these materials have shown good properties as supports for various metals and other catalytic active species. These mesoporous materials are regarded as excellent catalyst supports for active metallic particles due to their high surface area, uniform pore size and pore volume, and thermal stability.[8–10] Santa Barbara amorphous (SBA)-15 itself does not show substantial catalytic activity, unless appropriate active metal species are impregnated inside SBA-15.[9] SBA-15 has been extensively used in the field of catalysis due to its good hydrothermal stability resulting from its thicker pore walls.[11,12]

Few authors have previously synthesized copper-containing SBA-15. They used Cu/SBA-15 for different applications such as steam reforming, hydroxylation, partial oxidation, complete oxidation, and so forth.[8,11,13–23] Table 1 shows a comparative assessment on characterization of Cu/SBA-15 and its applications. It may be seen in Table 1 that Cu/SBA-15 has never been used for CWPO of any recalcitrant compound like pyridine. Moreover, most of previous researchers did not characterize the catalyst Cu/SBA-15 after its potential use and did not report on its reusability, which is very essential considering the high cost of SBA-15. Table 2

Additional Supporting Information may be found in the online version of this article.

Correspondence concerning this article should be addressed to V.C. Srivastava at vimalcsr@yahoo.co.in.

Table 1. Literature Review of Synthesis of Cu/SBA-15 for Various Applications

Characterization technique and application	Wang et al.[11] Cu/SBA-15	Tu et al.[13] Cu/SBA-15	Carrero et al.[14] Cu-Ni/SBA-15	Karvana and Atakül[15] Cu/SBA-15	Habimana et al.[16] Ni/Cu/SBA-15	Chen et al.[8] Cu/SBA-15	Calles et al.[17] CuNi/CeO_2/SBA-15 and CuNi/La_2O_3/SBA-15	Wang et al.[18] Cu-Fe/SBA-15	Patel et al.[19] Cu/SBA-15	Bardajee et al.[20] $CuBr_2$/SBA-15	Prathap et al.[21] Cu/SBA-15	Sorolla et al.[22] Cu-TiO_2/SBA-15	Zhang et al.[23] Cu/SBA-15	This work Cu/SBA-15
XRD	X	X	X	X	X	X	X	X	X	X	X	X	X	X
BET	X	X	X	X	X	X	X	X	X	X	X	X		X
FE/SEM											X			X
FTIR	X					X		X						X
TPR		X	X		X	X	X		X					X
TGA							X	X					X	
ICP-AES/AAS	X		X			X	X	X		X			X	X
TEM		X	X		X	X	X	X		X	X	X	X	
Process	Hydroxylation of phenol	CO oxidation	Ethanol steam reforming	Desulfurization	Partial oxidation of methane	Hydrogenolysis of dimethyl maleate	Ethanol Steam reforming	Carbonylation of methanol	Selective catalytic reduction of NO	Synthesis	Sensing of glucose	Photocatalytic degradation of paraquat	Phenol hydroxylation	Wet peroxidation of pyridine
End products	Catechol and hydroquinone	CO_2, H_2, H_2O	Hydrogen production		Syn gas	1,4-butanediol	Hydrogen	Dimethyl carbonate		Pyridopyrazine and quinoxaline			Diphenol, catechol, hydroquinone	

X denotes that particular study reported in that study.
XRD: X-ray diffraction; TGA: Thermo-gravimetric analysis; ICP: inductively coupled plasma; AES: atomic emission spectroscopy; AAS: Atomic absorption spectroscopy; TEM: Transmission electron microscopy.

shows various oxidation methods for the treatment of pyridine bearing wastewater.[2,3,24–26] Although each technology has its own drawbacks, CWPO is promising technology that has emerged as a feasible substitute technology for the treatment of medium to high organic loading wastewater using hydrogen peroxide as the oxidant.

To the best of the knowledge of the authors, CWPO of pyridine bearing wastewater by any type of catalyst is not reported earlier. In this study, Cu was dispersed in SBA-15, and this synthesized Cu/SBA-15 was characterized by various techniques. The main aim of this article was to optimize the operating parameters such as copper loading wt %, pH, catalyst dose, H_2O_2 dose, and temperature for the CWPO of pyridine present in aqueous solution by Cu/SBA-15. Kinetics and thermodynamics of the process have also been explored, and catalyst recyclability for the CWPO of pyridine has been checked.

Materials and Methods

Materials

All the chemicals used in the study were of analytical reagent grade. Tetraethylorthosilicate (TEOS; Aldrich, Germany), pluronic P123 (PEO20-PPO70-PEO20, Aldrich, Germany), copper sulfate (S.D. fine chemicals, India), pyridine (S.D. fine chemicals, India), HCl (Ranken, India), 30 wt % hydrogen peroxide (Ranken, India), and so forth were purchased from various companies.

Synthesis of catalyst and its characterization

SBA-15 was synthesized in two steps.[27] First, 4 g of pluronic P123 was dispersed in 150 mL of HCl (2 M) with continuous stirring. The solution was heated to 40°C over a water bath, and 9 mL of TEOS was added drop-wise with constant stirring. The mixture was sealed in a polypropylene bottle, stirred at 40°C for 24 h, and then hydrothermally heated at 90°C under static conditions for another 24 h. The solid product was washed with deionized water and dried at 100°C overnight. Then, the calcination of the materials was done at 550°C in air for 6 h so as to remove P123 templates. The calcined samples were designated as SBA-15. $CuSO_4{\cdot}7H_2O$ was used as the precursor of Cu ion. Required amount of copper precursor was dissolved in double distilled water so as to obtain different wt % Cu solutions. These solutions were agitated along with requisite amount of SBA-15 for 3 h so as to obtain 5, 10, and 20 wt % Cu on the prepared SBA-15. The reaction mixture was twice hydrothermally heated at 100°C under static condition for 12 h each, and then, the samples were calcined at 550°C for 6 h. The calcined sample was designated as Cu/SBA-15.

The textural properties of the samples were analyzed by N_2 adsorption–desorption isotherms obtained at 77 K using Micromeritics ASAP 2020 apparatus. Before the analysis, the sample was degassed at 300°C for ≈6 h. The surface area was obtained using Brunauer–Emmett–Teller (BET) model for adsorption data in a relative pressure range of 0.05–0.30. The total pore volumes were calculated from the amount of N_2 vapor adsorbed at a relative pressure of 0.99. The average pore diameter of samples was determined by assuming that all pores in the sample are parallel and cylindrical, by dividing the pore volume with the surface area.

Fourier transform infrared (FTIR) spectra was obtained over a range of 4000–400 cm^{-1} with a Nicolet Avatar 370

Table 2. Various Oxidation Methods of Pyridine Bearing Wastewater

System	Supporting Materials	Catalyst	Type of Rector	Temperature, Pressure, pH	Initial Conc. (mg/L)	Reaction Time (min)	Degradation (%)	References
Catalytic oxidation	Zeolite, MCM-41, γ-Al_2O_3	Cu	Microreactor	250–700°C, normal	600	30	100%	Zhou et al.[24]
Catalytic wet air oxidation	Carbon	Cu-Co, $CuSO_4$	Stainless steel reactor	140–160°C, 9 bar, 4-pH	10	90	64%	Chaudhary et al.[3]
Catalytic oxidation	γ-Al_2O_3	Pt		350–520°C	0.1–0.85% vol.			Ismagilov et al.[25]
Fenton's oxidation		Iron	1-L glass beaker	1–4 pH	COD 60,000 and 23,000 mg/L	240	62.2% COD	Padoley et al.[2]
Fenton's oxidation		Iron	500-mL glass beaker	2–4 pH	12,500	120	74.0% COD	Bag et al.[26]
Photo assisted Fenton's		Iron		2–4 pH			67.0% COD	Bag et al.[26]
Photocatalysis		TiO_2		4 pH				Bag et al.[26]
Wet peroxidation	SBA-15	Cu/SBA-15	250-mL oil bath reactor	85°C, at natural pH	100	300	97% conversion of PY, 92% TOC	This study

CSI spectrometer (Thermo Electrom Corporation). The sample to be characterized was grounded using KBr pellet technique.

Temperature-programmed reduction (TPR) experiments were performed out on a Micromeritics AutoChem 2920 equipment. For this, 25 mg of catalyst was loaded into a U-shape quartz reactor, and sample was degasified with argon (20 mL/min) at 200°C for 2 h to remove physisorbed moisture. After cooling to room temperature, the gas was switched to 10% H_2 in argon flow (20 mL/min), and catalyst was heated to 800°C with a heating rate of 20°C/min. Effluent gas was passed through a cold trap to trap moisture in effluent gas before reaching the thermal conductivity detector (TCD). The amount of H_2 consumption during reduction was monitored by a TCD.

H_2-pulse chemisorptions were performed out on Micromeritics AutoChem 2920 equipment, using TCD detector. Before starting pulse chemisorptions, sample was degasified with argon at 200°C for 1 h and reduced in 10% H_2/Ar at 250°C for 1 h. After that the sample was flushed with argon for 1 h at 270°C and cooled down to 35°C in flowing argon. Hydrogen pulse chemisorption was started with catalyst at 35°C using loop gas hydrogen and repeated until the hydrogen peaks became identical.

To understand the morphology, a field emission scanning electron microscope (FE-SEM)/energy-dispersed X-ray spectra (EDX) QUANTA, Model 200 FEG was used. The samples were first grounded to make the samples homogeneous and then spread on sample holders in such a manner to produce flat surfaces. After this, the samples were gold coated using sputter coater (Edwards S150) to provide conductivity to the samples, and then, the images of FE-SEM were taken at an acceleration voltage of 20 kV under low vacuum, and then, EDX were taken to find metal content of sample. The error in the content of elements determined using this method is between 5 and 10%.

Experimentation

The experimental studies were carried out in a 250-mL three-necked round-bottomed glass reactor and equipped with a total reflux system. The total reflux prevented loss of pyridine vapor. Magnetic stirrer was used to agitate the mixture and keep the solution homogeneous during the experimentation. The temperature of the reaction mixture was raised using the hot-plate to the desired value, and it was kept constant during the experimental run using a proportional–integral–derivative controller. In each run, the reactor was charged with 100 mL pyridine solution of required concentration. The oil bath was then heated up and stabilized to the desired reaction temperature called time zero (time $t=0$ for the reaction was taken). When thermal equilibrium was reached, required amount of catalyst (Cu/SBA-15) and oxidation agent (hydrogen peroxide) was added to reaction mixture.

Analysis of pyridine concentration and total organic carbon

Pyridine concentration was monitored using high performance liquid chromatograph (HPLC) (Waters), with a C18 reverse phase column. The mobile phase was a mixture of 80% methanol and 20% distilled water and had a flow rate of 0.5 mL/min. Pyridine was detected and measured via UV absorbance at a wavelength of 254 nm. Meanwhile, the total organic carbon (TOC) was determined using TOC analyzer (Shimadzu TOC-V). The percentage removal of pyridine and TOC were calculated using the following equation

$$\text{Percentage removal}\,(X)=\left(\frac{C_o-C_t}{C_o}\right)\times 100 \qquad (1)$$

where C_o is the initial pyridine concentration (mg/L), and C_t is the pyridine concentration (mg/L) after time (t). All the experiments were done in triplicate, and results were found to show $\pm 5\%$ deviation from the average value. Reported results are average of three runs. The copper content of Cu/SBA-15 catalysts were analyzed by ion chromatography (IC) (Mehtrom) equipped with professional UV/VIS detector. The samples were digested in nitric acid and filtrated through membrane filter (0.25 μm).

Table 3. Textural Characteristics of the Copper-Containing Mesoporous Silica Materials

Sample	wt %	IC	S_{BET} (m^2/g)	V_p (cm^3/g)	D_p (nm)	$S_{Micropore}$ (m^2/g)
SBA-15			650	0.820	6.0	68.3
Cu/SBA-15	5	4.5	569	0.783	5.8	60.57
Cu/SBA-15	10	9.3	486	0.680	5.2	52.0
Cu/SBA-15	20	18.2	313	0.542	5.00	10.5

S_{BET}: BET surface area; V_p: total pore volumes were obtained at P/P_o=0.99; D_p: average pore diameter calculated by BJH method; and S_{BET}: *t*-plot micropore area.

Results and Discussion

Characterization

Nitrogen adsorption–desorption measurements were used to evaluate the textural properties of catalyst samples (SBA-15 and Cu/SBA-15), and the results are listed in Table 3. Nitrogen adsorption–desorption isotherms, shown in Figure 1a, of all the samples exhibited international union of pure and applied chemistry type IV-isotherms nature. All samples except 20 wt % SBA-15 exhibited a clear H1 hysteresis loops at high relative pressure as depicted in Figure 1a. However, 20 wt % Cu/SBA-15 showed H_2 type hysteresis loop corresponding to ink-bottle pores and reduction of the pore volume. The hysteresis loop of the Cu/SBA-15 was due to percolation effect caused by small Cu nanocrystals settling within the mesopores and effectively forming ink-bottle type pores.[28] As predictable, the presence of metal molecules leads to corresponding decrease in BET surface area, pore volume, and pore diameter in metal-containing SBA-15 signifying that a substantial amount of copper had been adsorbed on the pore walls of SBA-15 framework that did not block the mesopores.[29]

TPR is a powerful tool to study the reduction behavior of active phase and metal species in different states. TPR provides useful information about the redox property of a catalyst as well as the identification of different species. TPR profiles of Cu/SBA-15 sample with various copper loadings are shown in Figure 1b. Two main reduction peaks were observed with maximum around 560 and 640 K, respectively. The first peak may be assigned to reduction of Cu^{2+} to Cu^{+}, and the second peak may be assigned to subsequent reduction of Cu^{+} to Cu^{o} and Cu^{2+} to Cu^{o}. The relative intensity of the second peak increased with increase of Cu loading because of an increase in particle size of Cu as shown in Table 4. Similar behavior has been reported by Martínez et al.[30] for cobalt-loaded mesoporus silica. Generally, nonsupported copper reduction of bulk CuO to Cu^{o} is considered as one-step process at about 500 K.[31] In the case of supported CuO, reduction can occur in the range of 400–600 K, depending on the copper oxide dispersion and the nature of the support.[32] Generally, small particles are expected to get reduced at lower temperatures, and the bulk copper oxide is expected to get reduced at higher temperature.[33] H_2-TPR results (Figure 1b) confirm the formation of highly dispersed smaller copper species on the surface of SBA-15. Generally, reduction of well-dispersed CuO particles to Cu^{o} and reduction of copper phyllosilicate to Cu^{+} occurs at temperature of ~516 K. TPR profile of unloaded SBA-15 showed a straight line pattern, and no reduction peak was observed in the temperature range of 303–1073 K.

H_2-chemisorption study was carried out to determine metal distribution and active particle size. Metal dispersion was found to be 32.28, 7.05, and 1.12% for 5%Cu–SBA-15, 10% Cu–SBA-15, and 20% Cu–SBA-15, respectively. Respective active particle sizes were found to be 3.2, 99.3, and 845.6 nm. Thus, it may be seen that the metal dispersion decreased with an increase in copper loading, whereas the trend was opposite for active particle size. Tu et al.[13] also observed decrease in metal dispersion and an increase in active particle size with an increase in copper loading on supports. In this study, beyond 5% Cu loading on SBA-15, the particle size of Cu will become enlarged due to sintering.[13]

The FTIR spectrum of SBA-15 and Cu/SBA-15 shown in Figure 2 represents bands centered at 474, 811, 1073, and 1225 cm^{-1}, which are typical of Si—O—Si vibrations of SBA-15 silica framework.[34] The band at 1640 cm^{-1} is generally attributed to H—O—H banding vibrations of adsorbed water molecules.[32] The Cu-loaded SBA-15 samples showed a decrease in the intensity of the band at 960 cm^{-1} in comparison to parent SBA-15 silica. The peak at 629 cm^{-1},

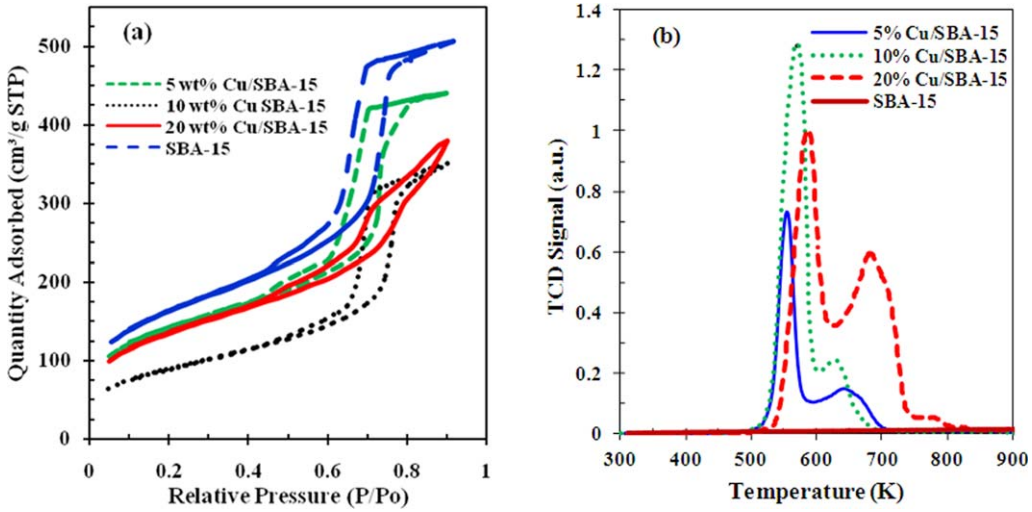

Figure 1. (a) Nitrogen adsorption desorption isotherms of SBA-15 and Cu/SBA-15 and (b) TPR profile of Cu-containing SBA-15.

[Color figure can be viewed in the online issue, which is available at wileyonlinelibrary.com.]

Table 4. Reducing Temperature Summary of the CuO/SBA-15 Catalysts

Sample	Temperature of Peak Maximum (K)		H_2 Consumption	H_2 Consumption
	T_{1max}	T_{2max}	(T_{1max})	(T_{2max})
SBA-15	–	–	–	–
5% Cu/SBA-15	560	640	43.8338	7.4904
10 wt % Cu/SBA-15	570	635	102.1880	5.4594
20 wt % Cu/SBA-15	585	680	99.8911	91.0743

which was attributed to the stretching of Cu(I)—O, confirmed the presence of Cu_2O.[35] This confirms Cu incorporation into the framework of SBA-15 and copper species to the silica surface with the formation of Si—O—Cu-type association.[34] The IR spectrum of the samples showed absence of Cu—O stretch vibration band at 536 cm^{-1}.[36]

The morphology of Cu on SBA-15 structure was analyzed using SEM images combined with the EDX analysis. SBA-15 and copper-containing SBA-15 samples possessed typical fiber-like morphology. Distribution of elements as shown in Figure 3 by EDX mapping indicates that the major elements in Cu/SBA-15 are carbon, oxygen, silica, and copper. The elemental mapping survey reveals that all elements were uniformly distributed throughout the samples.

Effect of Cu metal loading on SBA-15 for oxidation

First, catalytic activity of blank SBA-15 was tested for pyridine oxidation. At catalyst dose of 1 g/L, H_2O_2 dose of 2.3 mL/L, temperature of 358 K, and initial pyridine concentration of 100 mg/L, only 20% removal was observed with SBA-15. Aydemir et al.[9] reported that SBA-15 itself does not show substantial catalytic activity unless appropriate active metal species are impregnated inside SBA-15. The effect of Cu loading on pyridine oxidation was studied, and the results are shown in Figure 4a in terms of TOC removal. Catalytic activity first increased with Cu loading up to 10 wt %, though the difference in catalytic activity of 5 and 10% Cu-loaded SBA-15 was very marginal. However, pyridine removal efficiency decreased with an increase Cu loading beyond 10%. Tu et al.[13] reported that Cu particles having maximum dispersion capacity of 5 wt %. Beyond this value, the particles become enlarged due to sintering. And these large Cu particles are less active as compared to smaller particles. Dispersion of Cu metal on SBA-15 plays a key role due to possibility of Cu particles getting confined deep into the channels that may not participate in the oxidation reaction. Only those Cu particles that are positioned at or near the pore opening act as the reaction sites. Because of above reasons, 5 wt % Cu/SBA-15 was taken as optimum loading for CWPO of pyridine. This 5 wt % Cu/SBA-15 was used for further study to optimize various operating parameters.

Effect of pH

In oxidation process, pH of the solution plays vital role on removal efficiency for the oxidation of organic wastewater. In this study, pH of the pyridine-containing aqueous solution was varied in the range of 3–10. The reaction was carried out at 328 K for 6 h with a catalyst dose (Cu/SBA-15) of 1 g/L and 2.98 mL/L dose of 30 wt % of H_2O_2. The results are shown in Figure 5a in terms of pyridine and TOC removal. It clearly indicates that the degradation of the pyridine increases with an increase up to 7. Furthermore for pH>7, removal efficiencies decreased. The maximum pyridine removal was observed around neutral pH (6–7 pH). Similar results have been reported by various investigators using copper as active species.[37,38] The natural pH of 100 mg/L pyridine solution was 6.2–6.3. A near-neutral pH (or natural pH) condition is preferable due to ease of operation in large-scale industrial application. In addition, acidic conditions significantly enhance the leaching of active component from SBA-15 that is not desirable.[39] Considering these reasons, further studies were carried out at natural pH only.

Effect of catalyst dose

In this study, catalyst dose was varied in the range of 0.05–3 g/L, while the other parameters were kept constant (temperature=328 K, H_2O_2 dose=2.9 mL/L, and pyridine concentration=100 mg/L). The experimental results are shown in Figure 5b. It was observed that for Cu/SBA-15 dose>1 g/L, increase in removal efficiency is not significant. This phenomenon may be caused by several reasons. One reason is that due to the high catalytic activity (high surface area catalyst) the excessive catalyst may promote the decomposition of H_2O_2, resulting in lower utilization of H_2O_2.[35] Optimum catalyst dose of 1 g/L was used in subsequent studies.

Effect of the H_2O_2 dose

Amount of H_2O_2 in the solution is directly related to the number of hydroxyl radicals generated, which ultimately affects the removal efficiency. In this study, H_2O_2 dose was varied in the range of 0.96–3.85 mL/L. The catalyst dose was maintained at the observed optimum of 2 g/L of Cu/SBA-15, and pyridine concentration was 100 mg/L and temperature 328 K. It could be seen in Figure 5c that the pyridine removal increased with an increase in dose of

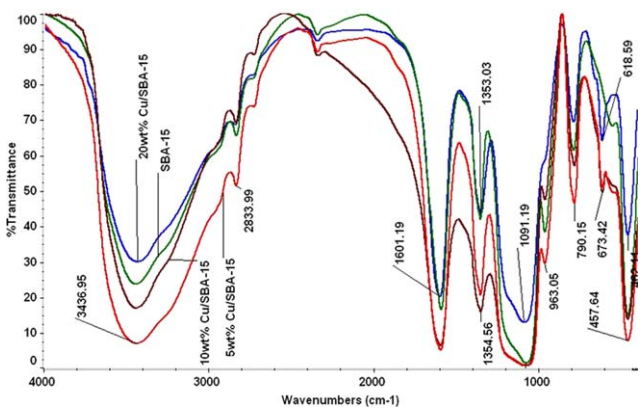

Figure 2. FTIR spectra of SBA-15 and Cu/SBA-15.

[Color figure can be viewed in the online issue, which is available at wileyonlinelibrary.com.]

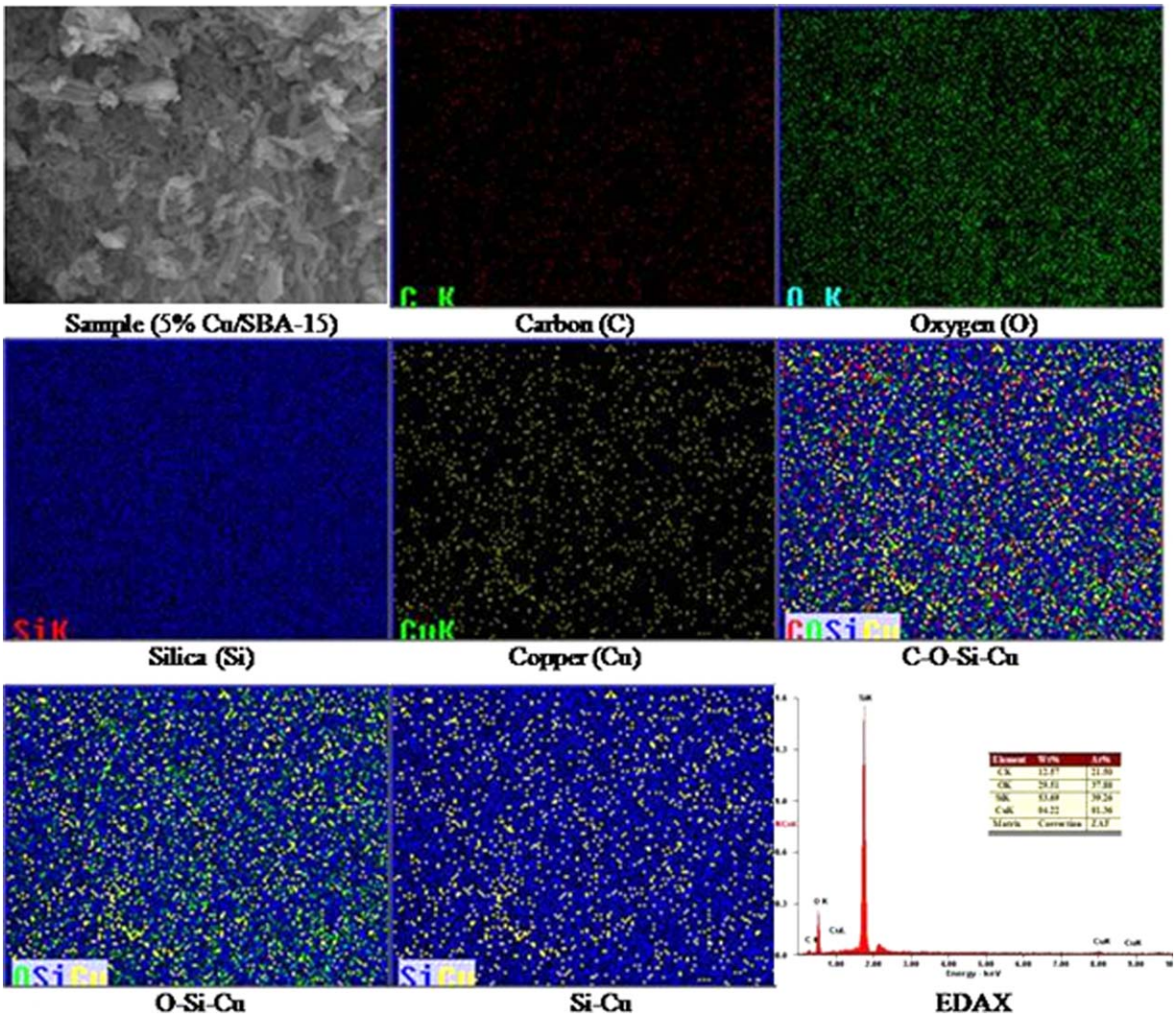

Figure 3. SEM/EDAX mapping of 5% Cu/SBA-15.

[Color figure can be viewed in the online issue, which is available at wileyonlinelibrary.com.]

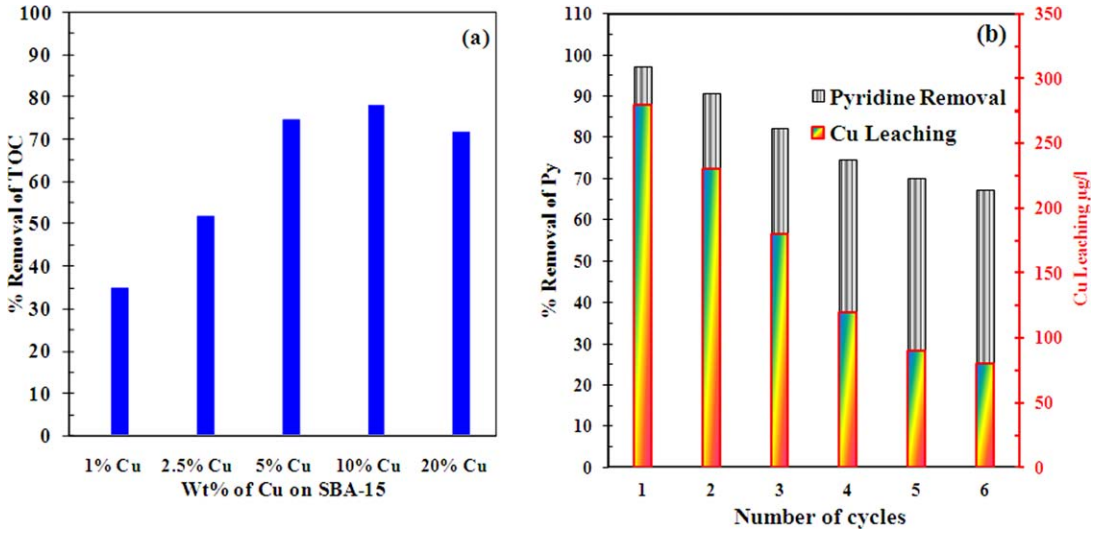

Figure 4. (a) Effect of metal loading on pyridine oxidation (T=328 K, H_2O_2=2.90 mL/L, Co=100 mg/L, Cu/SBA-15=1 g/L, and time=6 h) and (b) reusability and leaching study of Cu/SBA-15 (Cu/SBA-15 dose=1 g/L, H_2O_2=2.9 mL/l, Co=100 mg/L, and time=6 h).

[Color figure can be viewed in the online issue, which is available at wileyonlinelibrary.com.]

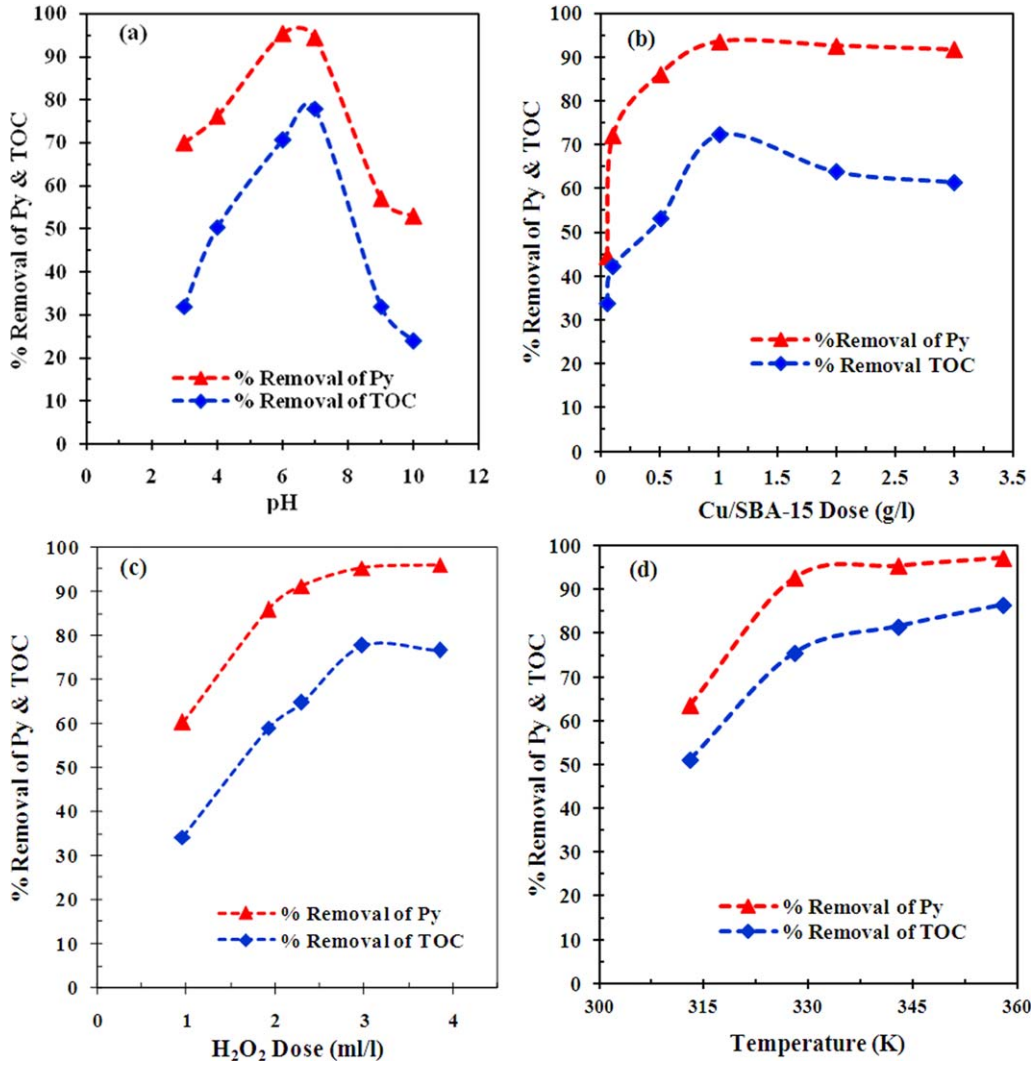

Figure 5. Effect of various variables on pyridine oxidation: (a) effect of pH (T=328 K, H_2O_2=2.90 mL/L, Co=100 mg/L, and Cu/SBA-15=1 g/L); (b) effect of catalyst dose (T=328 K, H_2O_2=2.9 mL/L, and Co=100 mg/L); (c) effect of H_2O_2 dose (T=328 K, Cu/SBA-15 dose=1 g/L, and Co=100 mg/L); and (d) effect of temperature (Cu/SBA-15 dose=1 g/L, H_2O_2=2.3 mL/L, and Co=100 mg/L).

[Color figure can be viewed in the online issue, which is available at wileyonlinelibrary.com.]

H_2O_2. Conversely, an excess amount of H_2O_2 addition (>3 mL/L) did not cause significant pyridine removal because of the self scavenging effect in which $HO^{\bullet}$ radicals combine together to form water.[40] Considering this, the optimum H_2O_2 dose of 3 mL/L was used so as to avoid build up of undesirable intermediates in the system.[2]

Effect of reaction temperature and kinetic study

The reaction temperature is a key operating parameter in CWPO. Pyridine removal was monitored by varying temperature in the range 313–358 K for pyridine oxidation by Cu/SBA-15 (Figure 5d). As expected, an increase in temperature enhanced the overall removal of pyridine. It can be seen from the figure that by increasing the temperature from 313 to 359 K, the pyridine removal increased from ~63 to ~97%. At high temperature (>343 K), the nature of reaction became very fast, and it reached reaction equilibrium within 2 h.

In the kinetic investigation, the CWPO of pyridine bearing wastewater under excess hydrogen peroxide content was studied so as to avoid the H_2O_2 dependence of the CWPO reaction kinetics. For a first-order reaction, the simplified kinetic rate expression can be expressed as

$$-\ln(C/C_o)=kt \tag{2}$$

where k is first-order reaction rate constant, t is the time, C is pyridine concentration at any time t, and C_o is the initial pyridine concentration. Slope of $\ln(C_o/C)$ vs. t (Figure 6) gives the value of the reaction rate constant at different temperatures. Apparently, two-stage first-order reaction kinetics describes the pyridine peroxidation. The nature of obtained curves at different temperatures are similar (Figure 6), that is, fast reaction for the initial 45 min duration and followed by slow reaction for the next 300 min. Values of the reaction rate constant were found for both steps at all temperatures (Table 5). The curves well fitted to the first-order kinetic with good coefficient of determination ($R^2 > 0.93$) values between the experimental and calculated values.

The activation energy (E) and the frequency factor (k_o) were determined for both steps (fast and slow steps) from

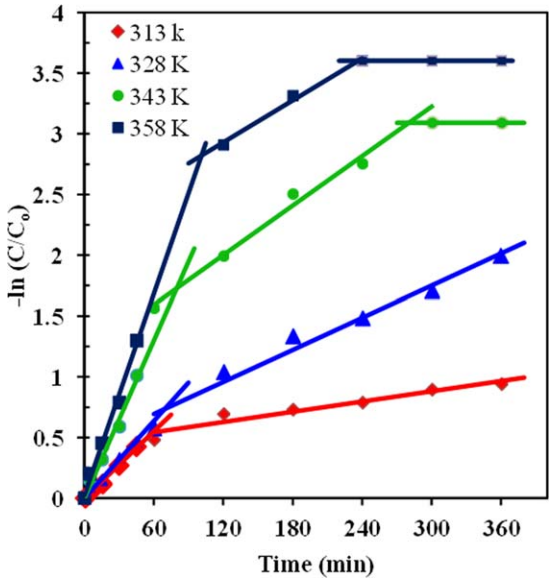

Figure 6. Determination of reaction rate constants in the two stages of the CWPO of pyridine performed at different temperatures (Cu/SBA-15 dose=1 g/L, H_2O_2=2.3 mL/L, and Co=100 mg/L).

[Color figure can be viewed in the online issue, which is available at wileyonlinelibrary.com.]

the obtained rate constants at different temperatures by Arrhenius equation given as follows

$$k = k_o e^{-E_a/\mathrm{RT}} \tag{3}$$

Values of E_a and k_o were obtained from the slope and intercept of Arrhenius plot (ln k vs. $1/T$ plot), respectively. The activation energy values were found to be 25.61 and 32.10 kJ/mol for fast and slow reaction steps, respectively. Values for frequency factor were found to be 150 and 325 min^{-1}, respectively.

Reusability of Cu/SBA-15 catalyst for oxidation of pyridine

The catalytic activity of Cu-SBA-15 catalyst was monitored over six runs of the reaction, and the results are presented in Figure 4b. The Cu/SBA-15 wrapped with the poly tetra fluoro ethylene (PTFE) membranes can effectively prevent loss of amorphous catalyst. In the recycling study, 100 mg of Cu/SBA-15 catalyst was wrapped in PTFE membrane. For this study, H_2O_2 dose was maintained at the observed optimum 3 mL/L, pyridine concentration was 100 mg/L, and temperature was kept constant at 328 K. After reaching desired temperature of reaction mixture, H_2O_2 and wrapped catalyst was added to the reaction solution. Pyridine removal decreased with each cycle, and more than 70% removal efficiency was observed after six runs. Wrapped Cu/SBA-15 catalyst retained high catalytic activity until six cycles, demonstrating the satisfactory reusability of the catalyst.

Cu leaching was also measured in each cycle using ion chromatograph equipped with UV/VIS detector. Cu leaching was always less than 210 μg/L, which is much less than 3 mg/L, permissible copper concentration for discharge of wastewater in India.[41]

Reaction mechanism of pyridine oxidation

The reaction path for the CWPO of pyridine involves catalyst reduction and $HO^{\bullet}$ radical generation as discussed in this section. It is well known that conversion of H_2O_2 molecules into hydroxyl radicals greatly promotes the degradation of organic compounds.[42] The active phase of transition metal ion reacts with H_2O_2, via reactions 4–6, leading to formation of peroxy radical (HO_2^-) and hydroxyl radical ($HO^{\bullet}$) which have high oxidation potential.[11] However, excess amount of active phase of copper on the catalyst also converts peroxy radical (HO_2^-) to nascent oxygen by reaction 7. In addition, in presence of an excess amount of H_2O_2, $HO^{\bullet}$ radicals combined together to form water via reaction Eqs. 8 and 9.[40]

$$\mathrm{Cu}^{2+}/\mathrm{SBA\text{-}15} + \mathrm{H_2O_2} \rightarrow \mathrm{Cu}^{+}/\mathrm{SBA\text{-}15} + \mathrm{H}^{+} + \mathrm{HO_2}^{-} \tag{4}$$

$$\mathrm{Cu}^{+}/\mathrm{SBA\text{-}15} + \mathrm{H_2O_2} \rightarrow \mathrm{Cu}^{2+}/\mathrm{SBA\text{-}15} + HO^{\bullet} + \mathrm{OH}^{-} \tag{5}$$

$$\mathrm{Cu}^{+}/\mathrm{SBA\text{-}15} + \mathrm{H_2O_2} + \mathrm{H}^{+} \rightarrow \mathrm{Cu}^{2+}/\mathrm{SBA\text{-}15} + HO^{\bullet} + H_2O \tag{6}$$

$$\mathrm{Cu}^{2+}/\mathrm{SBA\text{-}15} + \mathrm{HO_2}^{-} \rightarrow \mathrm{Cu}^{+}/\mathrm{SBA\text{-}15} + \mathrm{O}^{2-} + \mathrm{H}^{+} \tag{7}$$

$$HO^{\bullet} + H_2O_2 \rightarrow HO_2^{\bullet} + H_2O \tag{8}$$

$$HO^{\bullet} + HO_2^{\bullet} \rightarrow O_2 + H_2O \tag{9}$$

$$H^{+} + \mathrm{OH}^{-} \rightarrow H_2O \tag{10}$$

$HO^{\bullet}$ radicals formed during above reactions react with pyridine to finally convert it N_2, CO_2, and H_2O. During pyridine oxidation, many intermediates such as ammonia, dimethylamine, formic acid, acetic acid, glutaconic acid, and oxalic acid may get formed before complete mineralization.[24] The reaction mechanism for the CWPO of pyridine via formation of intermediates is described in Figure 7. Organic acids (acetic acid, formic acid, oxalic acid, and glutaconic acid) were analyzed using ion chromatograph for experimental run conducted at optimum condition (catalyst dose=1 g/L, H_2O_2 dose (30%)=2.3 mL/L, temperature=358 K, and initial pyridine concentration=100 mg/L). Formic acid, acetic acid, and oxalic acid were found to be present at concentrations <2 mg/L; however, glutaconic acid was not detected. Ion chromatograph was also used for determining the concentration of various nitrogenous compounds during pyridine mineralization. Ammonia (3.5 mg/L), nitrates (3.0

Table 5. Kinetic and Thermodynamic Parameters for the Pyridine Removal

Temperature (K)	Fast Step				Slow Step			
	K (1/min)	R^2	E_a (kJ/mol)	k_o (1/min)	K (1/min)	R^2	E_a (kJ/mol)	k_o (1/min)
313	0.009	0.99	25.61	150.65	0.001	0.92	32.10	325.38
328	0.010	0.98			0.004	0.97		
343	0.021	0.98			0.005	0.94		
358	0.028	0.99			0.005	0.74		

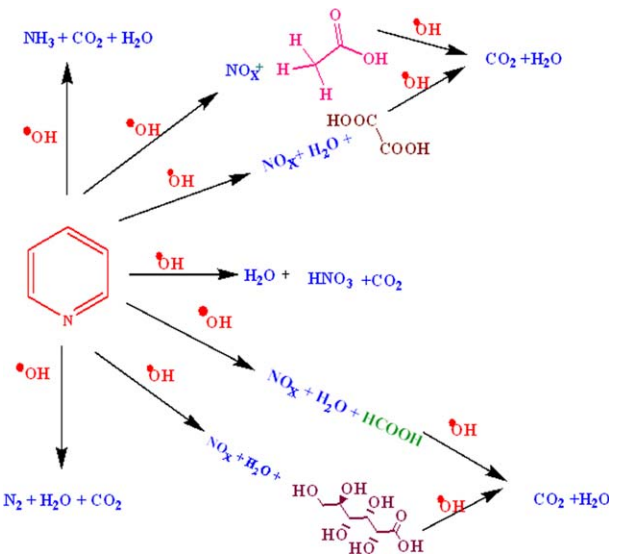

Figure 7. Possible reaction mechanism pathways during CWPO of pyridine.

[Color figure can be viewed in the online issue, which is available at wileyonlinelibrary.com.]

mg/L), nitric acid (2.0 mg/L), and nitrites (0.5 mg/L) were detected in the sample. Thus, by nitrogen balance, 70% of the total nitrogen in pyridine gets converted to nitrogen gas.

Conclusions

In this study, a series of copper-containing SBA-15 materials have been synthesized via impregnation technique. Cu-loaded SBA-15 showed potential capacity for catalytic oxidation of pyridine bearing wastewater by hydrogen peroxide as oxidant. Cu incorporation into the framework of silica tetrahedral was confirmed by various characterization (BET, FE-SEM, EDX, FTIR, and TPR) studies. Results showed that 5 wt % Cu/SBA-15 exhibited best catalytic activity. Maximum CWPO of pyridine was found to happen at 358 K with Cu/SBA-15 dose of 1 g/L, H_2O_2 (30 wt %) dose of 2.3 mL/L with reaction time of 3 h. Cu/SBA-15 (5 wt %) showed good operational stability during recycling test with high removal and low copper leaching. The CWPO mechanism for complete mineralization of pyridine was also explained.

Literature Cited

1. Niu J, Conway BE. Development of techniques for purification of waste waters: removal of pyridine from aqueous solution by adsorption at high-area C-cloth electrodes using in situ optical spectrometry. *J Electroanal Chem*. 2002;52:16–28.
2. Padoley KV, Mudliar SN, Banerjee SK, Deshmukh SC, Pandey RA. Fenton oxidation: a pretreatment option for improved biological treatment of pyridine and 3-cyanopyridine plant wastewater. *Chem Eng J*. 2011;166:1–9.
3. Chaudhary RR, Kumar P, Chand S. Catalytic wet air oxidation of toxic nitrogen containing (pyridine) from wastewater. *J Sci Ind Res*. 2006;65:757–759.
4. Bermejo MD, Cocero MJ. Supercritical water oxidation: a technical review. *AIChE J*. 2006;52:11:3933–3951.
5. Crowther N, Larachi F. Iron-containing silicalites for phenol catalytic wet peroxidation. *Appl Catal A*. 2003;46:293–305.
6. Plant L, Jeff M. Hydrogen peroxide: a potent force to destroy organics in wastewater. *Chem Eng*. 1994;101:6–20.
7. Perathoner S, Centi G. Wet hydrogen peroxide catalytic oxidation (WHPCO) of organic waste in agro-food and industrial streams. *Top Catal*. 2005;33:207–224.
8. Chen LF, Hartmann PJ, Zhu LJ, Qiao MH, Shen W, Xu HL, Fan KN. Preparation of Cu/SBA-15 catalysts by different methods for the hydrogenolysis of dimethyl maleate to 1,4-butanediol. *Appl Catal A*. 2009;356:129–136.
9. Aydemir B, Sezgi NA, Dogu T. Synthesis of TPA impregnated SBA-15 catalysts and their performance in polyethylene degradation reaction. *AIChE J*. 2012;58:2466–2472.
10. Deshpande PA, Polisetti S, Madras G, Jyothi D, Chandrasekaran S. Dispersed ZrO_2 Nanoparticles in MCM-48 with high adsorption activity. *AIChE J*. 2012;58:2987–2996.
11. Wang L, Kong A, Chen B, Ding H, Shan Y, He M. Direct synthesis, characterization of Cu-SBA-15 and its high catalytic activity in hydroxylation of phenol by H_2O_2. *J Mol Catal A*. 2005;230:143–150.
12. Marugan J, Grieken RV, Alfano OM, Cassano AE. Optical and physicochemical properties of silica-supported TiO_2 photocatalysts. *AIChE J*. 2006;52:2832–2843.
13. Tu CH, Wang AQ, Zheng MY, Wang XD, Zhang T. Factors influencing the catalytic activity of SBA-15-supported copper nanoparticles in CO oxidation. *Appl Catal A*. 2006;297:40–47.
14. Carrero A, Calles JA, Vizcaıno AJ. Hydrogen production by ethanol steam reforming over Cu-Ni/SBA-15 supported catalysts prepared by direct synthesis and impregnation. *Appl Catal A*. 2007;327:82–94.
15. Karvana O, Atakül H. Investigation of CuO/mesoporous SBA-15 sorbents for hot gas desulfurization. *Fuel Process Technol*. 2008;89:908–915.
16. Habimana F, Li X, Ji S, Lang B, Sun D, Li C. Effect of Cu promoter on Ni-based SBA-15 catalysts for partial oxidation of methane to syngas. *J Nat Gas Chem*. 2009;18:392–398.
17. Calles JA, Carrero A, Vizcaíno AJ. Ce and La modification of mesoporous Cu–Ni/SBA-15 catalysts for hydrogen production through ethanol steam reforming. *Micropor Mesopor Mater*. 2009;119:200–207.
18. Wang H, Wang B, Liu CL, Dong WS, Oxidative carbonylation of methanol over copper ion-containing ionic liquids immobilized on SBA-15. *Micropor Mesopor Mater*. 2010;134:51–57.
19. Patel A, Rufford TE, Rudolph V, Zhu Z. Selective catalytic reduction of NO by CO over CuO supported on SBA-15: effect of CuO loading on the activity of catalysts. *Catal Today*. 2011;166:188–193.
20. Bardajee GR, Malakooti R, Jami F, Parsaei Z, Atashin H. Covalent anchoring of copper-Schiff base complex into SBA-15 as a heterogeneous catalyst for the synthesis of pyridopyrazine and quinoxaline derivatives. *Catal Commun*. 2012;27:49–53.
21. Prathap MUA, Kaur B, Srivastava R. Direct synthesis of metal oxide incorporated mesoporous SBA-15, and their applications in non-enzymatic sensing of glucose. *J Colloid Interface Sci*. 2012;381:143–151.
22. Sorolla MG, Dalida ML, Khemthong P, Grisdanurak N. Photocatalytic degradation of paraquat using nano-sized Cu–TiO_2/SBA-15 under UV and visible light. *J Environ Sci*. 2012;24:1125–1132.
23. Zhang H, Tang C, Lv Y, Sun C, Gao F, Dong L, Chen Y. Synthesis, characterization, and catalytic performance of copper-containing SBA-15 in the phenol hydroxylation. *J Colloid Interface Sci*. 2012;380:16–24.
24. Zhou J, Xia QH, Shen SC, Kawi S, Hidajat K. Catalytic oxidation of pyridine on the supported copper catalysts in the presence of excess oxygen. *J Catal*. 2004;225:128–137.
25. Ismagilov ZR, Kerzhentsev MA, Besedin VI, Susharina TL. Formation of nitrogen oxides in catalytic oxidation of pyridine. *React Kinet Catal Lett*. 1983:23:43–48.
26. Bag BC, Sai M, Sekhar K, Bhattacharya C. Treatment of wastewater containing pyridine released from n,n′-dichlorobis (2,4,6-trichlorophenyl) urea (CC2) plant by advanced oxidation. *J Environ Protect Sci*. 2009:3:34–40.
27. Zhao D, Huo Q, Feng J, Chmelka BF, Stucky GD. Nonionic triblock and stardiblock copolymer and oligomeric surfactant synthesis of highly ordered, hydrothermally stable, mesoporous silica structures. *J Am Chem Soc*. 1998;120:6024–6036.
28. Landau MV, Vradman L, Wang X, Titelman L. High loading TiO_2 and ZrO_2 nanocrystals ensembles inside the mesopores of SBA-15: preparation, texture and stability. *Micropor Mesopor Mater*. 2005;78:117–129.
29. Chen S, Lee J, Cheng S. Pinacol-type rearrangement catalyzed by Zr-incorporated SBA-15. *J Catal*. 2010;270:196–205.
30. Martínez A, López C, Márquez F, Díaz I. Fischer-Tropsch synthesis of hydrocarbons over mesoporous Co/SBA-15 catalysts: the

influence of metal loading, cobalt precursor, and promoters. *J Catal*. 2003;220:486–499.
31. Hartmann M, Racouchot S, Bischof C. Characterization of copper and zinc containing MCM-41 and MCM-48 mesoporous molecular sieves by temperature programmed reduction and carbon monoxide adsorption. *Micropor Mesopor Mater*. 1999;27:309–320.
32. Velu S, Wang L, Okazaki M, Suzuki K, Tomura S. Characterization of MCM-41 mesoporous molecular sieves containing copper and zinc and their catalytic performance in the selective oxidation of alcohols to aldehydes. *Micropor Mesopor Mater*. 2002;54:113–126.
33. Hartmann X, Yin A, Dai WL, Fan K. One pot synthesis of ultrahigh copper contented Cu/SBA-15 material as excellent catalyst in the hydrogenation of dimethyl oxalate to ethylene glycol. *Catal Lett*. 2009;132:22–27.
34. Zhang L, Zhao Y, Dai H, He H, Au CT. A comparative investigation on the properties of Cr-SBA-15 and CrOx/SBA-15. *Catal Today*. 2008;131:42–54.
35. Zhan Y, Zhoua X, Fua B, Chen Y. Catalytic wet peroxide oxidation of azo dye (Direct Blue 15) using solvothermally synthesized copper hydroxide nitrate as catalyst. *J Hazard Mater*. 2011;187:348–354.
36. Garcia-Cuello VS, Giraldo L, Moreno-Piraj JC. Synthesis, characterization, and application in the CO oxidation over a copper nanocatalyst confined in SBA-15. *J Chem Eng Data*. 2011;56:1167–1173.
37. Fathima NN, Aravindhan R, Rao JR, Nair BU. Dye house wastewater treatment through advanced oxidation process using Cu-exchanged Y zeolite: a heterogeneous catalytic approach. *Chemosphere*. 2008;70:1146–1151.
38. Zhan Y, Li H, Chen Y. Copper hydroxyphosphate as catalyst for the wet hydrogen peroxide oxidation of azo dyes. *J Hazard Mater*. 2010;180:481–485.
39. Granato T, Katovic A, Valkaj KM, Tagarelli A, Giordano G. Cu-silicalite-1 catalyst for the wet hydrogen peroxide oxidation of phenol. *J Porous Mater*. 2009;16:227–232.
40. Dhananjeyan MR, Mielczarski E, Thampi KR, Buffat P, Bensimon M, Kulik A, Mielczarski J, Kiwi J. Photodynamics and surface characterization of TiO_2 and Fe_2O_3 photocatalysts immobilized on modified polyethylene films. *J Phys Chem B*. 2001;105:12046–12055.
41. CPCB. Pollution Control Acts, Rules and Notification Thereunder. India: Central Pollution Control Board, 2001.
42. Inchaurrondo N, Cechini J, Font J, Haure P. Strategies for enhanced CWPO of phenol solutions. *Appl Catal B*. 2011;111–112:641–648.

Manuscript received July 16, 2012, and revision received Nov. 17, 2012.